Modelling the Complete DTIN Killchain: A Comparative Study of Laser and Kinetic Effectors with RADAR Detection Against Small Drones in Counter-UAS Scenarios

Alexandre Heuchamps[a, †], François Harmel[b, †], Marijke Vandewal[b], and Alexandre Papy[a]

[a]Department of Weapon Systems and Ballistics, Royal Military Academy, 30 Avenue de la Renaissance, Brussels, Belgium
[b]Department of Communications, Information, Systems and Sensors, Royal Military Academy, 30 Avenue de la Renaissance, Brussels, Belgium
[†]These authors contributed equally

ABSTRACT

Unmanned aerial systems (UAS) and unmanned aerial vehicles (UAV), commonly known as drones, are increasingly being used in both civil and military contexts. The advances in embedded computing power are enabling some UAS to operate fully autonomously, posing significant challenges to existing countermeasures. In response to this evolving threat landscape, directed energy weapon (DEW) technologies, including high energy lasers (HEL), are emerging as promising solutions in the counter-UAS (C-UAS) domain to complement kinetic means. This is due to their low cost per shot, virtually unlimited ammunition capacity, speed-of-light engagement, high accuracy level, and scalability of on-target effects tailored to the UAS threat level. This study aims to evaluate the effectiveness and performance of HEL technology as a killchain-integrated C-UAS solution in various scenarios, using modelling and simulation, and comparing those to what could be obtained by using kinetic effectors. Such performance is obtained by integrating simplified representations of UAS with parametric HEL and kinetic effector models. This paper contributes to ongoing efforts to improve security measures against the escalating threat of drone proliferation in today's dynamic and complex environments.

Keywords: HEL, C-UAS, Modelling, Killchain, Performance

1. INTRODUCTION

The lowest part of NATO class 1[1] unmanned aircraft systems (UAS) are low, slow, and small (LSS) flying devices. The combination of minimal signatures, low-speed and altitude flights, with their multi-mission capabilities, low cost, and wide proliferation makes them an attractive asset to both state[2,3,4,5] and non-state[6,7,8,9] actors. In response to the escalating threat posed by those UAS, dedicated countermeasures have been developed, often presenting limited performance against small UAS (sUAS) compared to organic weapon systems.[10,11] The current developments in software and embedded computing power now enable swarms of LSS UAS to fly fully autonomously,[12,13,14,15,16] creating additional strain on existing counter-sUAS (C-sUAS) systems.

Recognising the threat level escalation posed by sUAS, and the limitations of traditional UAS countermeasures, some nations, including the United States of America, China, and Russia, have been investing in the development of directed energy weapon (DEW) systems,[17,18] including high energy lasers (HEL). According to its government accountability office, the United States of America spent on average 1 billion USD annually on DEW development efforts,[19] highlighting the potential of such technologies for counter-drone applications. Offering near speed-of-light engagement, combined with high accuracy, low cost per shot, deep magazine, and scalability of on-target effects, HEL weapons have the potential to flip the current negative cost exchange ratio of traditional C-sUAS systems.

Despite their appealing advantages and the deployment of some prototypes for realistic in-field testing,[20] HEL still face several challenges, including their limitation to line of sight (LOS) engagements, their performance degradation in unfavourable weather conditions,[21,22] the self-induced performance degradation due to thermal

Send correspondence to Alexandre Heuchamps (e-mail: alexandre.heuchamps@mil.be)

High-Power Lasers and Technologies for Optical Countermeasures II, edited by Willy L. Bohn, Marc Eichhorn, Gareth D. Lewis, Proc. of SPIE Vol. 13201, 1320108 · © 2024 SPIE · 0277-786X · doi: 10.1117/12.3031432

blooming,[23] the difficulty to obtain high beam quality and higher output power,[24] and the lack of understanding on how those weapon systems would perform in a given scenario. This paper addresses the final point through a comparative analysis of the performance of HEL systems, when integrated into a C-sUAS killchain, against kinetic effectors within a specified scenario. To do so, section 2 presents first the model for the sUAS, with relevant parameters, in section 2.1.1, the models used for the sensors and effectors used to detect, track, identify, and neutralise (DTI-N) sUAS in sections 2.1.2 to 2.1.4, and typical scenarios where sUAS are used in section 2.2. The initial stages of the DTI-N killchain utilise RADAR, which is modelled using either the RADAR range equation or the Shnidman equation, both discussed in section 2.1.2. The final stage, neutralisation, is executed using either a HEL, presented in section 2.1.3 or a kinetic effector, presented in section 2.1.4, which trajectory is computed through either a point mass model (PMM) or a modified PMM (MPMM). Section 2.2 introduces typical scenarios that might occur in C-sUAS settings, with an emphasis on intelligence, information, and surveillance (ISR) applications, and on direct attack. Section 3 explains the methodology by which the various models outlined in section 2.1 are integrated within a killchain, and details the mechanisms through which information is transmitted between its successive components. Section 4 presents the challenges encountered to model the killchain, and gives, wherever applicable, clues on how to mitigate those challenges. Finally, section 5 concludes this work and proposes a way ahead for parametric performance studies applied to HEL in C-sUAS settings.

2. MODELS, HYPOTHESES, AND SCENARIOS

To replicate the scenarios presented in section 2.2, practical and usable representations for both the target sUAS and the sensors and effectors employed within the DTI-N killchain steps have to be established. The definitions of these models, along with the foundational assumptions, are expounded in section 2.1. Specifically, section 2.1.1 describes the sUAS model, section 2.1.2 will present the different RADAR models used for the DTI parts of the killchain, whereas sections 2.1.3 and 2.1.4 focus on the HEL and kinetic effector models, respectively.

2.1 Models and Hypotheses

2.1.1 sUAS

While sUAS present a big variability is both shapes and sizes, they all present the same general trend, where one dimension is much smaller than the other two.[25] Consequently, in the remainder of this work, target sUAS are modelled as single-body ellipsoids made up of a single homogeneous isotropic material, where the three main radii are confounded with principal rotation axes. The chosen representation presents several advantages over a parallelepipedic configuration, out of which two stand out particularly. First, an ellipsoidal representation discards edge effects, considerably simplifying several aspects linked to target-HEL interactions, such as on-target HEL beam projection. Second, an ellipsoid can be degenerated into a sphere if the application allows it, inducing perfect rotational symmetry, drastically reducing the required computational power to represent the target compared to a full mesh. The sUAS flightpath, i.e. its trajectory over time, is parametrised by a series of waypoints through which the ellipsoid centre passes, with associated timestamps.

2.1.2 RADAR Sensor

RADAR relies on the propagation of radio waves to detect (successive) positions of (airborne) targets. Typically operating in the microwave region of the electromagnetic spectrum, the wavelengths at play are of the same order of magnitude as LSS UAS geometrical dimensions. Moreover, sUAS present reduced RADAR cross section (RCS) signatures, usually of about 1 cm^2,[26] making their detection, tracking, and identification challenging for traditional C-UAS RADAR systems. In practice, a radar C-sUAS system is often used for detection and is combined with another technology, such as an EO sensor, which identifies targets previously detected by the radar. However, for the purposes of this paper, it is assumed that the radar alone is perfectly capable of handling the DTI stages of the killchain, as will be developed in section 3.2.

Different complexity models exist to model C-UAS RADAR systems performance. For the purposes of this article, it was decided to develop a basic model based on the RADAR range equation and a more advanced model based on the Shnidman equation. These two models give an estimate of the range at which detection can be

performed. The advanced model gives additional information about the probability of detecting the target at a given distance. The RADAR equation gives a maximum detection range $R_{\max}$[27]

$$R_{\max} = \sqrt[4]{\frac{\sigma \lambda^2 n_{\text{pulses}} \mathcal{G}_{\text{RX}} \mathcal{G}_{\text{TX}} \mathcal{P}_{\text{TX}}}{(4\pi)^3 \, \text{MDS}}},$$

where σ is the (frequency, polarisation, position and orientation independent) target RCS, λ the RADAR wavelength, n_{pulses} the number of pulses emitted by the RADAR, $\mathcal{G}_{\text{TX}}$ (resp. $\mathcal{G}_{\text{RX}}$) the transmitter (resp. receiver) antenna gain, $\mathcal{P}_{\text{TX}}$ the RADAR emitted power, and MDS the minimum discernable signal, i.e. the critical power under which an echo cannot be discriminated with the background noise. As that quantity can rarely be assessed, it can be substituted by the thermal (white Gaussian) noise $\mathcal{P}_n$, and the signal to noise ratio (SNR), yielding

$$R_{\max} = \sqrt[4]{\frac{\sigma \lambda^2 n_{\text{pulses}} \mathcal{G}_{\text{RX}} \mathcal{G}_{\text{TX}} \mathcal{P}_{\text{TX}}}{\text{SNR} \, (4\pi)^3 \, T_0 k_B B F}},$$

where, in addition to the terms introduced previously, the Boltzmann constant k_B, the standard temperature T_0, and the receiver noise figure F and instantaneous bandwidth B, respectively, have been included. In practice, the SNR is hardly available and is accounted for through a random variable X_{SNR} which, per Shnidman's equation,[28] is approximated by

$$X_{\text{SNR}} = C \frac{X_\infty}{n_{\text{pulses}}},$$

where C is empirically calculated by combining the probability of detection $\Pr(\text{detection})$, the probability of false alarm $\Pr(\text{false alarm})$, n_{pulses}, and the appropriately selected Swerling constant K. Similarly, X_∞ is empirically calculated by combining $\Pr(\text{detection})$, $\Pr(\text{false alarm})$, and n_{pulses}, under the hypothesis of noncoherent integration of n_{pulses}.

2.1.3 High Energy Laser Effector

Applying the paraxial approximation to the Cartesian wave equation yields Hermitte-Gaussian (HG) beams, described by the product of Hermitte polynomials with Gaussian functions.[29,30] At the lowest order, those transverse electromagnetic (TEM) propagation modes degenerate into pure Gaussian beams, which contracts to a minimum diameter at the beam waist w_0, before expanding passed that location.[31] The opto-thermo-mechanical coupling existing between a HEL and an illuminated target drives the damage the former inflicts on the later, and is dictated by the interaction of several parameters, such as target constitutive material and fluence damage thresholds, HEL power P_{HEL}, wavelength λ and pulse parameters, dwell time t_{dwell}, beam quality M^2, and angular spreading Θ_{spread}. Parameters linked either to targets or HEL are considered constant in the remaining of this paper. Furthermore, the full heat equation is not solved. The total angular beam spread can be written as $\Theta_{\text{spread}} = \sqrt{\Theta_{\text{diff}}^2 + \Theta_{M^2}^2 + \Theta_{\text{jitter}}^2 + \Theta_{\text{atmosphere}}^2}$, where $\Theta_{\text{diff}} = \frac{\lambda}{\pi w_0}$ is the angular spread of a diffraction-limited Gaussian beam, $\Theta_{M^2} = \left(M^2 - 1\right) \Theta_{\text{diff}}$ is the angular spread of higher order modes due to finite beam quality, Θ_{jitter} is the angular spread due to beam jitter, and $\Theta_{\text{atmosphere}}^2 = \Theta_{\text{turbulence}}^2 + \Theta_{\text{blooming}}^2$ is the angular spread due to the atmospheric propagation, consisting of a turbulence-induced spread $\Theta_{\text{turbulence}}^2$ and a thermal blooming-induced part $\Theta_{\text{blooming}}^2$, all counted relative to the propagation direction. Under the assumption of moderate turbulence, i.e. when beam speckling is negligible, the turbulence-induced beam spreading takes the form $\Theta_{\text{turbulence}} = \frac{2}{k \rho_0}$ with

$$\rho_0 = \begin{cases} \infty & \text{for } z < z_c, \\ \left(0.5 k^2 C_N^2 z\right)^{-3/5} & \text{for } z_c < z < z_i, \\ \left(0.76 z^{1/2} C_N l_0^{-1/6} k\right)^{-1} & \text{for } z > z_i, \end{cases}$$

the radial coherence length, C_N^2 the refractive index structure constant of the turbulence, l_0 and L_0 the inner and outer turbulence scale size, respectively, k a constant, and z_c and z_i length scales given by

$$z_c = \left(0.4 k^2 C_N^2 L_0^{5/3}\right)^{-1} \text{ and } z_i = \left(0.4 k^2 C_N^2 l_0^{5/3}\right)^{-1}.$$

The beam spread due to thermal blooming takes the form $\Theta^2_{\text{blooming}} = C_B P^a_{\text{HEL}}$, where a is a constant greater than 1, equal to 1.1777 for a uniform beam, and C_B is a dimensionless constant. In Cartesian coordinates, for a higher-order TEM HG beam travelling in the z direction, the time-averaged HEL irradiance intensity is modelled through the relation[32,33]

$$I(x,y,z) = I_0 \left[\frac{w_0}{w(z)}\right]^2 H_m^2\left[\sqrt{2}\frac{x}{w(z)}\right] H_n^2\left[\sqrt{2}\frac{y}{w(z)}\right] \exp\left[-2\frac{x^2+y^2}{w^2(z)}\right], \tag{1}$$

where $I_0 = \frac{2P_{\text{HEL}}}{\pi w_0^2}$ is the HEL peak irradiance, x and y are orthonormal coordinates axes defining a plane with normal along z, and $H_m(x)$ the order m Hermitte polynomial. Considering no cross-influence between the different spreading factors, the time-averaged laser spot size, measured at a distance z from w_0, is given by

$$w^2(z) = z^2\left[\left(M^2\Theta_{\text{diff}}\right)^2 + \Theta_{M^2} + \Theta^2_{\text{jitter}} + \Theta^2_{\text{turbulence}} + \Theta^2_{\text{blooming}}\right]. \tag{2}$$

2.1.4 Kinetic Effector

Although limited to LOS engagement, and unlike HEL, kinetic effectors offer a non-immediate, non-scalable, target engagement, with trajectories impacted by external parameters such as wind. The effector trajectory can be computed through different models with increasing complexity levels. Amongst these models, the PMM and MPMM are considered. The first considers a perfectly stable projectile as a point where all the (constant) mass is concentrated, hence no rotational or aerodynamic effects other than the drag are considered. Under such hypotheses, the projectile motion is described by[34]

$$m_{\text{proj}}\frac{\mathrm{d}^2}{\mathrm{d}t^2}\boldsymbol{x}_{\text{proj}} = m_{\text{proj}}\boldsymbol{g} - \frac{1}{2}\rho S_{\text{proj}} C_{D_0} \|\boldsymbol{v}_{\text{proj}}\| \boldsymbol{v}_{\text{proj}}, \tag{3}$$

where m_{proj}, $\boldsymbol{x}_{\text{proj}}$, $\boldsymbol{v}_{\text{proj}}$, and S_{proj} represent the projectile's mass, position, velocity (relative to the ground), and surface (conventionally replaced by $S_{\text{proj}} = \frac{\pi d^2}{4}$, with d the projectile's calibre), respectively, $\boldsymbol{g}$ and ρ represent the (constant) gravity acceleration and medium density, respectively, and C_{D_0} the Mach number-dependent projectile drag coefficient, which expression can be approximated with

$$C_{D_0} = \begin{cases} C^\star_{D_0} & \text{for Ma} \leq 1 \\ \frac{k}{\text{Ma}^n}\ (k \in \mathbb{R}^+, n \in \mathbb{R}^+) & \text{for Ma} > 1. \end{cases}$$

Wind can easily be taken into account by considering $\boldsymbol{v} = \boldsymbol{v}_{\text{proj}} - \boldsymbol{v}_{\text{wind}}$ instead of simply $\boldsymbol{v}_{\text{proj}}$, in the right hand-side of equation (3), where $\boldsymbol{v}_{\text{wind}}$ is the wind velocity. An additional correction factor can be further included to consider projectile drift. In the framework of the MPMM, considering the projectile as a solid of revolution, effects linked its spin, such as spin damping and overturning moments, and Magnus force, are taken into account, in addition to the effects already considered in the PMM. Consequently, the yaw of repose in both trajectory and lateral planes is taken into account. For a dynamically-stable projectile modelled as a solid of revolution, the MPMM equations of motion read[35,36]

$$\begin{aligned} m_{\text{proj}}\frac{\mathrm{d}^2}{\mathrm{d}t^2}\boldsymbol{x}_{\text{proj}} =& m_{\text{proj}}(\boldsymbol{g} + \boldsymbol{\Lambda}) \\ &- \frac{1}{2}\rho S_{\text{proj}}\left(C_{D_0} + C_{D_{\alpha^2}}\|\boldsymbol{\alpha_e}\|^2\right)\|\boldsymbol{v}\|\boldsymbol{v} \\ &+ \frac{1}{2}\rho S_{\text{proj}}\|\boldsymbol{v}\|^2\left(C_{L_\alpha} + C_{L_{\alpha^3}}\|\boldsymbol{\alpha_e}\|^2\right)\boldsymbol{\alpha_e} \\ &- \frac{1}{2}\rho S_{\text{proj}} p d C_{\text{Mag-f}}(\boldsymbol{\alpha_e}\times\boldsymbol{v}) \end{aligned} \tag{4}$$

$$I_x\frac{\mathrm{d}}{\mathrm{d}t}p = \frac{1}{2}\rho S_{\text{proj}} p d^2 C_{\text{spin}}\|\boldsymbol{v}\|, \tag{5}$$

where equations (4) and (5) represent the projectile translation and rotation motions, respectively. In addition to the terms already defined in the PMM, the Coriolis acceleration $\boldsymbol{\Lambda}$, the induced drag force coefficient $C_{D_{\alpha^2}}$,

the lift force coefficient C_{L_α}, the cubic lift force coefficient $C_{L_{\alpha^3}}$, the Magnus force coefficient $C_{\text{Mag-f}}$, the axial inertia moment I_x, the angular velocity of the spinning motion p, and the spin damping coefficient C_{spin} have been included, together with the yaw of repose vector $\boldsymbol{\alpha}_e$, computed through the relation

$$\frac{1}{2}\rho S_{\text{proj}} d \left\|\boldsymbol{v}\right\|^2 \left(C_{M_\alpha} + C_{M_{\alpha^3}} \left\|\boldsymbol{\alpha}_e\right\|^2\right) \boldsymbol{\alpha}_e = -I_x p \frac{\boldsymbol{v} \times \left(\frac{\mathrm{d}}{\mathrm{d}t}\boldsymbol{v}_{\text{proj}}\right)}{\left\|\boldsymbol{v}\right\|^2},$$

where C_{M_α} and $C_{M_{\alpha^3}}$ are the overturning and cubic overturning moment coefficients, respectively. To model the interaction with a target sUAS, the v_{50} parameter, representing the speed at which a projectile has a 50% chance of target perforation,[37] can be taken into account.

2.2 Scenarios

Based on an open-access drone incident/attack database,[38] figure 1 has been constructed to illustrate both the sectors most impacted by sUAS and the principal missions they execute. According to figure 1a, airports are the

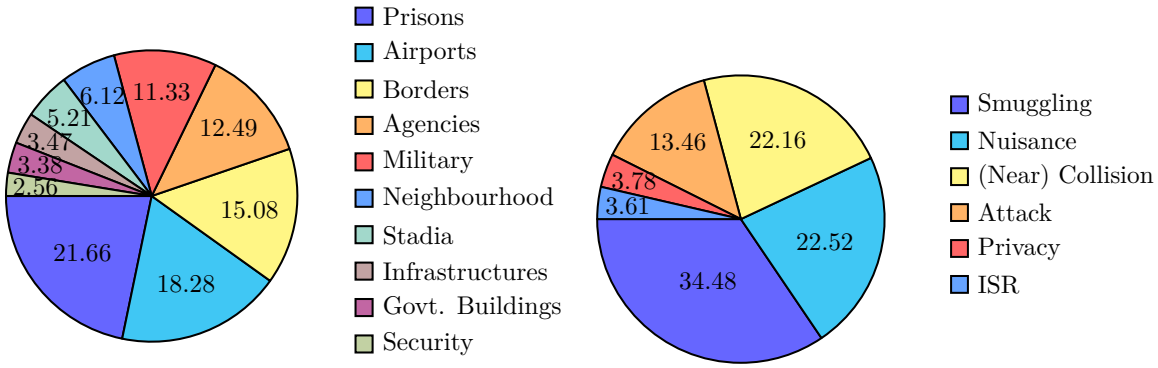

(a) Sectors (b) Missions

Figure 1: (a) Sectors, and (b) missions occurring the most in typical drone scenarios, based on the D-Fend Solutions database, spanning the period from 1st January to the 26th August 2024.[38] Figures expressed in percentage (rounding errors make the sums different from 100%).

most frequent theatres for drone incidents. However, since the specifics of airports are not discussed in this work, they are substituted by a generic asset around which different areas with varying security levels are established,[39] namely (a) layer L1, representing the distance at which camera-equipped sUAS could perform ISR missions. In that layer, any threat identified as a drone will be engaged by an effector, and (b) layer L2, representing the distance at which an explosive-laden drone could jeopardise the protected asset. In layer L2, any entering body is engaged, irrespective of whether or not it was identified as a threat. Both ISR and attack scenarios have been selected based on their relevance for real-world applications.[40] In the following, irrespective of the selected scenario and prevailing drone threat, only one effector is chosen to (potentially) engage a threat, facilitating performance comparison within the same scenario using the other effector.

3. METHODOLOGY

This sections establishes a connection between the models introduced in section 2.1 and the scenarios presented in section 2.2. It details the information flow along the killchain between the sensor, effector, target, and simulation code, as illustrated in figure 2, along with the different input/output parameters. In particular, section 3.1 focuses on the target sUAS, section 3.2 focuses on the RADAR, sections 3.3 and 3.4 deal with the HEL and kinetic effector, respectively, and section 3.5 tackles the simulation.

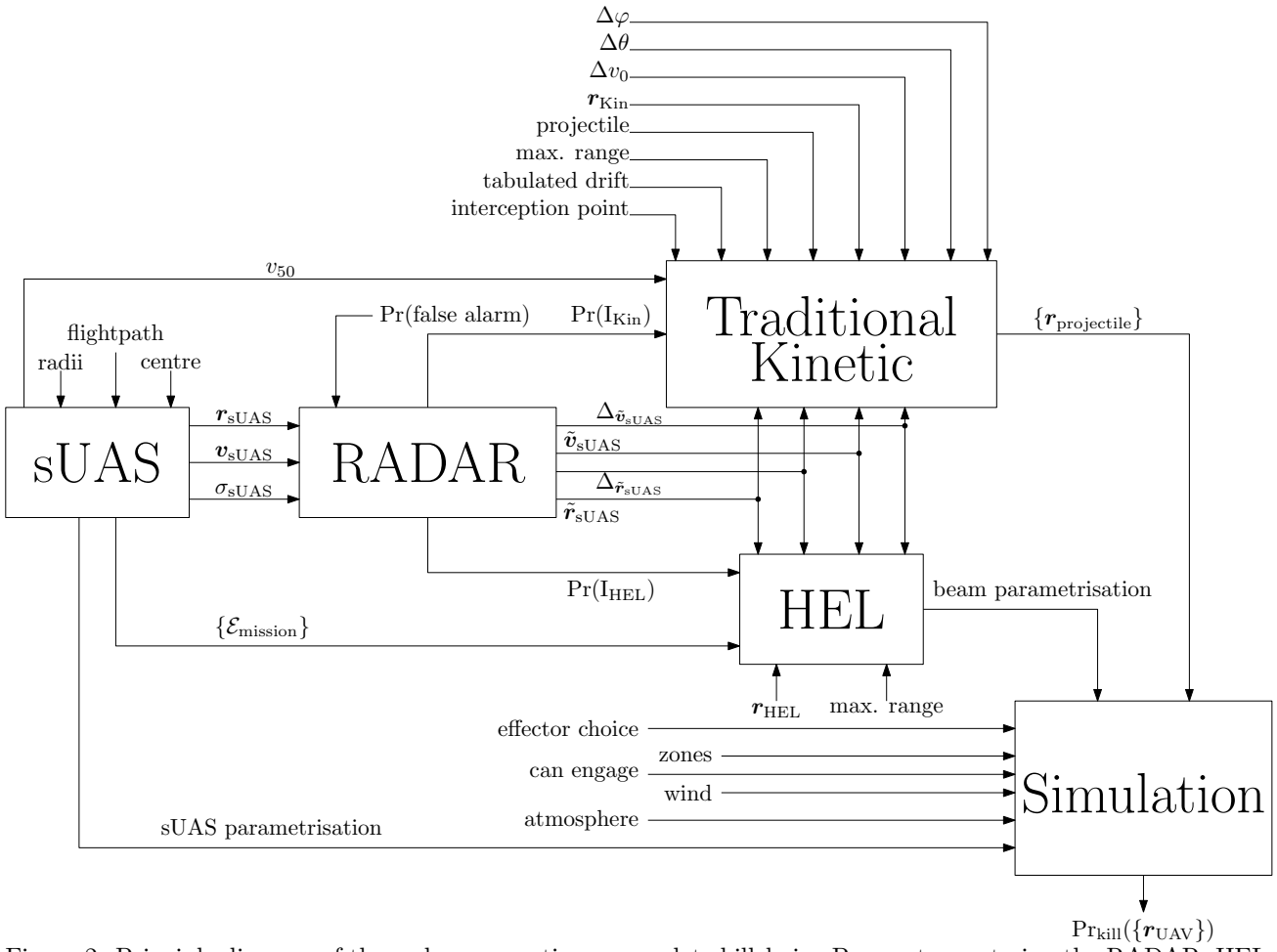

Figure 2: Principle diagram of the code representing a complete killchain. Parameters entering the RADAR, HEL, kinetic effector, sUAS, and simulation parts are given, together with how information flows between these parts.

3.1 UAV Methodology

As previously discussed, sUAS are modelled as single-body uniform ellipsoids, with their centres following a predetermined flightpath. The sUAS parametrisation is defined by four quantities: a centre, representing the ellipsoid's central position in 3D space, and the three principal radii of the ellipsoid, selected to mimic realistic target sUAS dimensions. General drone parameters, such as mass m and RCS are sourced from a specific database compiled from open-access industry datasheets. Several energy density thresholds, represented by $\{\mathcal{E}_{\text{mission}}\}$ in figure 2, are extracted from the drone and fed to the HEL model to specify the energy density thresholds at which the drone mission can no longer be successfully completed. The sUAS position $\boldsymbol{r}_{\text{sUAS}}$, velocity $\boldsymbol{v}_{\text{sUAS}}$, and RCS σ_{sUAS} are fed to the RADAR model, while its v_{50} is fed to the kinetic effector model.

3.2 RADAR Methodology

In addition to the target RCS, both RADAR models presented in section 2.1.2 require the target's position $\boldsymbol{r}_{\text{sUAS}}$ to perform the needed calculations: in the RADAR range equation, $\boldsymbol{r}_{\text{sUAS}}$ is used to check whether the target is within the sensor's detection area, while the advanced model requires both $\boldsymbol{r}_{\text{sUAS}}$ and Pr(false alarm) to compute the Pr(detection) associated with the target-sensor distance. After being detected, a body has to be identified as a sUAS. Considering a perfect RADAR in this work, the identification probability Pr(identification) is strictly equal to Pr(detection), hence any flying drone can be identified, and the HEL or kinetic effector get the same identification probability. Within the killchain, a delay between detection and identification events exists, linked to several sources, such as data acquisition or processing time needed for data fusion. Such delays are emulated by introducing approximations and errors on both the sUAS position and velocity, i.e. $\tilde{\boldsymbol{r}}_{\text{sUAS}}$, $\tilde{\boldsymbol{v}}_{\text{sUAS}}$, $\Delta_{\tilde{\boldsymbol{r}}_{\text{sUAS}}}$, and $\Delta_{\tilde{\boldsymbol{v}}_{\text{sUAS}}}$, respectively, which are fed to the used effector to specify the current position and velocity.

3.3 Kinetic Effector Methodology

Figure 2 enumerates some parameters not included in equations (3) to (5). Specifically, the "projectile" entry puts together the various aerodynamic coefficients, S_{proj}, and d. Additionally, errors in the initial launch azimuth, elevation, and ejection speed $\Delta\theta$, $\Delta\varphi$, and Δv_0 are considered, along with the successive launching platform positions $\boldsymbol{r}_{\text{Kin}}$ in case of a moving platform. For the remainder of this work, the platform is assumed to be static. A potential drift correction factor is also input, together with a constrained interception point, which must lie within both the sensor detection area and the maximum range distance, extracted from open-source literature.[41] By integrating these parameters with the previously introduced ballistics models, a projectile trajectory $\{\boldsymbol{r}_{\text{projectile}}\}$ is obtained, which is subsequently fed to the simulation component of the code.

3.4 HEL Methodology

Akin to the discussion in section 3.3, both positions for the HEL $\boldsymbol{r}_{\text{HEL}}$ and the maximum range for that effector are present, with the same meaning as previously, except applied to the HEL. The restriction on the maximum range is the same as previously, namely a target can be engaged only if it is within the RADAR detection area and at range for the HEL, which can be extracted from open publications.[42] The parametrisation of the HEL through the different equations introduced in section 2.1.3 is fed to the simulation block, where the interactions with the target are computed.

3.5 Simulation Methodology

The part of the code responsible for the simulation combines information from the chosen effector, the scenario, and the scene in which it is played. In particular, the different layers introduced previously are considered, together with atmospheric conditions and wind, as those influence the effector performance. An additional input, "can engage" in figure 2, is added to take into account potential collateral damage considerations: indeed, even if a sUAS meets the conditions to be engaged, the target-missing projectiles, or reflected HEL beam, could land in an undesired area. The output of the simulation is a kill probability for a target along its flightpath. This kill probability is computed based on the results provided by the different effectors. There are several ways of calculating a kill probability for an effector. For the purpose of this article, it was decided to compare the speed of the projectile with the reference velocity v_{50} to assess the kill probability linked to the kinetic effector. On the other hand, an energy accumulation was calculated for that linked to the HEL effector. The drone is considered

to have been taken down when this kill probability is greater than a certain threshold, specific to each scenario. This probabilistic approach highlights the importance of choosing a good threshold value, which will dictate when the effectors will be operational. For instance, if the constraint is too high, the effectors may act too late and the protected asset may suffer damage from the drone.

4. CHALLENGES AND DISCUSSION

Modelling the intricate interactions between sensors and/or effectors with a target for performance evaluation purposes presents a number of challenges at various levels, some of which are set out in this section. Throughout the modelling process, several difficulties emerged, which will be examined in detail. Furthermore, wherever possible, suggestions will be provided to facilitate the circumvention of these challenges. The specifics about RADAR are first presented in section 4.1, where it will be highlighted that more reality-fidelic results could be obtained if hypotheses on target RCS were relaxed. Next, HEL is discussed in section 4.2, with an emphasis on the difficulty of obtaining data for certain parameters, together with those encountered in linking all the equations and methodology described in sections 2.1.3 and 3, respectively. Finally, difficulties linked to kinetic effectors will be addressed in section 4.3.

4.1 RADAR Challenges

One of the biggest challenges with RADAR is to acquire realistic data for the frequency, polarisation, position and orientation dependent target RCS. Obtaining an open-source 4π sr RCS spectrum proves extremely challenging. Fortunately, some computer techniques, algorithms[43,44,45] and codes can be developed to evaluate parametrically a target RCS, even if numerical results can differ quite substantially from experimental results.[46,47] Common software packages dealing with RCS measurements include (but are not limited to) CST STUDIO SUITE,[48] FEKO,[49] XFDTD[50] and ANSYS HFSS.[51] This difficulty is practically discarded by considering statistically-averaged RCS values to model a given target, yielding decreased yet satisfactory performance[52,53] in most cases. Another challenging aspect of dealing with RADAR is their potential interaction: when two RADAR operate in overlapping frequency bands, interference might happen.[54] Although important, such interactions are considered as being de-conflicted in the present work, as a single radar sensor is used to perform the DTI tasks.

4.2 High Energy Laser Challenges

The difficulties to model HEL are manifold, and span different areas. First, obtaining values for some parameters such as the beam waist w_0, beam quality M^2, or jitter remain very difficult from literature alone. A possible way to get around is to contact companies manufacturing such effectors, even if they seldom provide the asked-for information. Another alternative consists in measuring those parameters, through either direct measurements,[55,56,57,58,59] or through the development of computer codes to automatically infer the value of different parameters knowing the conditions in which experiments were performed,[60] even if the parameters that can be inferred do not cover all those appearing in the different components of equations (1) and (2). Atmospheric effects modelling are another major difficulty, as an accurate representation would require heavy computational fluid dynamics simulations. Fortunately, advances in computational methods and power have enabled such codes to be developed.[61,62,63,64] Consequently, having a meaningful Θ_{spread}, thus a meaningful beam radius, is reachable, although conditional to being able to link with several other, external, software. Additionally, computing the intersection of the HEL beam with the target and assigning the right irradiance at each point of that intersection proves challenging.

4.3 Kinetic Effector Challenges

The principal difficulties when modelling kinetic effectors arise when the different aerodynamic coefficients appearing in equations (3) and (4) have to be determined. As for HEL, some values might be given by companies upon reasonable request, but more often than not nothing will get disclosed. Fortunately, different methods, either experimental or numerical, allow for the determination of the necessary values. Experimentally, coefficients can be extracted from firing tables or through live firing in dedicated areas, such as firing corridors or shooting ranges. Numerically, several codes, including (but not limited to) PRODAS,[65] ARFDAS,[66] or BALCO[67] have been developed to compute projectile trajectories. The seamless integration of such codes with the one used for

HEL models into a single environment adds an additional layer of complexity to the overall software development. Another difficulty arise from the data regarding azimuth, elevation, and ejection speed errors, as those are typically very difficult to obtain. Some users might nevertheless get some useful information by contacting manufacturers.

5. CONCLUSION

This work examined some difficulties one might encounter when a complete DTI-N C-sUAS killchain is to be modelled. By first presenting parametric models for both a RADAR used as sensor and a HEL or kinetic effector used for the neutralisation part of the killchain, and by then articulating how those interact together and with a target, clues are proposed to lessen or circumvent some of the encountered difficulties. This work should be considered as exploratory, and gives warning and hints to people wanting to address some of the challenges posed by sUAS.

ACKNOWLEDGMENTS

We thank the Royal Higher Institute for Defence (RHID) and the Ministry of Defence of Belgium for supporting this research within the DAP 22/12 Project.

REFERENCES

[1] JAPCC, [*A Comprehensive Approach to Countering Unmanned Aircraft Systems*], Joint Air Power Competence Centre, 15th year anniversary ed. (January 2021).

[2] Lowther, A. and Siddiki, M. K., "Combat Drones in Ukraine," *Air & Space Operations Review* **1**, 3–13 (December 2022).

[3] Chávez, K. and Swed, O., "Emulating underdogs: Tactical drones in the Russia-Ukraine war," *Contemporary Security Policy* **43**, 1–14 (September 2023).

[4] Kunertova, D., "The war in Ukraine shows the game-changing effect of drones depends on the game," *Bulletin of the Atomic Scientists* **79**, 95–102 (March 2023).

[5] Kunertova, D., "Drones have boots: Learning from Russia's war in Ukraine," *Contemporary Security Policy* **43**, 1–16 (October 2023).

[6] Rossiter, A., "Drone usage by militant groups: exploring variation in adoption," *Defense & Security Analysis* **34**, 113–126 (June 2018).

[7] Chávez, K. and Swed, O., "Off the Shelf: The Violent Nonstate Actor Drone Threat," *Air & Space Power Journal* **34**, 29–43 (September 2020).

[8] Chávez, K. and Swed, O., "The proliferation of drones to violent nonstate actors," *Defence Studies* **21**, 1–24 (November 2021).

[9] Haugstvedt, H., "A Flying Reign of Terror? The Who, Where, When, What, and How of Non-state Actors and Armed Drones," *Journal of Human Security* **19**, 1–7 (February 2023).

[10] NATO, "Comparative Analysis of Lethal, Low Collateral Damage Effectors Against Low, Small and Slow UAV," Report AC/344(C-UAS WG)D(2022)0001, North Atlantic Treaty Organization (September 2022).

[11] Papy, A., Ameloot, C., and Robbe, C., "Experimental Study of C-(s)UAS Detection and Neutralization Capabilities of in a Realistic Environment," in [*Proceedings - 33rd International Symposium on Ballistics, BALLISTICS 2023*], Coghe, F., ed., **1**, 835–844, DEStech Publications (October 2023).

[12] von Mammen, S., Tomforde, S., Höhner, J., Lehner, P., Förschner, L., Hiemer, A., Nicola, M., and Blickling, P., "OCbotics: An organic computing approach to collaborative robotic swarms," in [*2014 IEEE Symposium on Swarm Intelligence*], Jr., O. C. and Pozo, A., eds., **1**, 1–8, Institute of Electrical and Electronics Engineers (IEEE) (December 2014).

[13] Zhou, Y., Rao, B., and Wang, W., "UAV Swarm Intelligence: Recent Advances and Future Trends," *IEEE Access* **8**, 183856–183878 (October 2020).

[14] Skorobogatov, G., Barrado, C., and Salamí, E., "Multiple UAV Systems: A Survey," *Unmanned Systems* **8**, 149–169 (April 2020).

[15] Lehto, M. and Hutchinson, W. B., "Mini-drones swarms and their potential in conflict situations," in [*15th International Conference on Cyber Warfare and Security (ICCWS)*], Payne, B. K. and Wu, H., eds., **20**, 326–334, Academic Conferences Ltd (March 2020).
[16] Nathan, R. J. A. A., Kurmi, I., and Bimber, O., "Drone swarm strategy for the detection and tracking of occluded targets in complex environments," *Communications Engineering* **2**, 55 (August 2023).
[17] Sayler, K. M., "Defense Primer: Directed-Energy Weapons," Report IF11882, Congressional Research Service (February 2024).
[18] Sayler, K. M., "Emerging Military Technologies: Background and Issues for Congress," Report R46458, Congressional Research Service (February 2024).
[19] GAO, "Directed Energy Weapons: DOD Should Focus on Transition Planning," Report GAO-23-105868, United States Government Accountability Office (August 2023).
[20] Roque, A., "EXCLUSIVE: Strykers with 50-kilowatt lasers in CENTCOM for experiment, Army No. 2 says." Breaking Defense (March 2024). Available online at https://breakingdefense.com/2024/03/exclusive-strykers-with-50-kilowatt-lasers-in-centcom-for-experiment-army-no-2-says/ (last accessed on March 29, 2024).
[21] Fante, R. L., "Electromagnetic beam propagation in turbulent media," *Proceedings of the IEEE* **63**, 1669–1692 (December 1975).
[22] Fleck, J. A., Morris, J. R., and Feit, M. D., "Time-dependent propagation of high energy laser beams through the atmosphere," *Applied physics* **10**, 129–160 (June 1976).
[23] Smith, D., "High-power laser propagation: Thermal blooming," *Proceedings of the IEEE* **65**, 1679–1714 (December 1977).
[24] Varshney, A., Mainuddin, M., Singhal, G., and Nayak, J., "High power lasers for directed energy applications: Developments and challenges," *Infrared Physics & Technology* **136**, 105064 (January 2024).
[25] Saeed, A. S., Younes, A. B., Islam, S., Dias, J., Seneviratne, L., and Cai, G., "A review on the platform design, dynamic modeling and control of hybrid UAVs," in [*2015 International Conference on Unmanned Aircraft Systems (ICUAS)*], Valavanis, K. P., ed., **2**, 806–815, IEEE Robotics and Automation Society, Institute of Electrical and Electronics Engineers (IEEE) (June 2015).
[26] Patel, J. S., Fioranelli, F., and Anderson, D., "Review of radar classification and RCS characterisation techniques for small UAVs or drones," *IET Radar, Sonar & Navigation* **12**, 911–919 (July 2018).
[27] Richards, M. A., Scheer, J., Holm, W. A., and Melvin, W. L., [*Principles of Modern Radar*], SciTech Publishing, Incorporated (2010).
[28] Shnidman, D., "Determination of required SNR values [radar detection]," *IEEE Transactions on Aerospace and Electronic Systems* **38**, 1059–1064 (July 2002).
[29] Kogelnik, H. and Li, T., "Laser beams and resonators," *Proceedings of the IEEE* **54**, 1312–1329 (October 1966).
[30] Kogelnik, H., "On the Propagation of Gaussian Beams of Light Through Lenslike Media Including those with a Loss or Gain Variation," *Applied Optics* **4**, 1562–1569 (December 1965).
[31] Self, S. A., "Focusing of spherical Gaussian beams," *Applied Optics* **22**, 658–661 (March 1983).
[32] Liu, X., Jiang, D., Zhang, Y., Kong, L., Zeng, Q., and Qin, K., "Propagation Characteristics of Hermite–Gaussian Beam under Pointing Error in Free Space," *Photonics* **9** (July 2022).
[33] Hamed, A. M. and Al-Saeed, T. A., "Monte Carlo simulation of Hermite Gaussian laser beam in turbid medium," *Indian Journal of Physics* **98**, 357–364 (January 2024).
[34] McCoy, R. L., [*Modern Exterior Ballistics*], Schiffer Publishing Ltd., revised second ed. (March 1998).
[35] Lieske, R. F. and Reiter, M. L., "Equations of Motion for a Modified Point Mass Trajectory," Tech. Rep. AD0485869, Army Ballistic Research Lab, United States (March 1966).
[36] Baranowski, L., Majewski, P., and Szymonik, J., "Explicit form of the "modified point mass trajectory model" for the use in Fire Control Systems," *Bulletin of the Polish Academy of Sciences Technical Sciences* **68**, 1167–1175 (October 2020).
[37] Andres, C. and Boughers, W., "An Analysis of V50 Ballistic Limit Results Adjusting 1st Shot Velocity, Step-Up Step-Down Increments, Truth Characteristics and Velocity Control Distributions," Tech. Rep. ADA624217, Army Ballistic Research Lab, United States (March 2012).

[38] Solutions, D.-F., "Drone Attack & Incident Tracker," (February 2024).
[39] Maple, C. and Viduto, V., "A Visualisation Technique for the Identification of Security Threats in Networked Systems," in [*2010 14th International Conference Information Visualisation*], 551–556 (2010).
[40] Karlos, V. and Larcher, M., "Protection against Unmanned Aircraft Systems," Report KJ-NA-31-458-EN-C, European Commission (October 2023).
[41] Racek, F., Baláž, T., Krejčí, J., Procházka, S., and Macko, M., "Tracking, aiming, and hitting the UAV with ordinary assault rifle," in [*Counterterrorism, Crime Fighting, Forensics, and Surveillance Technologies*], Bouma, H., Carlysle-Davies, F., Stokes, R. J., and Yitzhaky, Y., eds., **10441**, 104410C, CENSIS: Innovation Centre for Sensor & Imaging Systems and Polish Technological Platform on Photonics and MIRPHAB and Photonics Society of Poland and Cranfield University, SPIE (September 2017).
[42] Kim, I. I., McArthur, B., and Korevaar, E. J., "Comparison of laser beam propagation at 785 nm and 1550 nm in fog and haze for optical wireless communications," in [*Optical wireless communications III*], Korevaar, E. J., ed., **4214**, 26–37, SPIE (February 2001).
[43] Yee, K., "Numerical solution of initial boundary value problems involving maxwell's equations in isotropic media," *IEEE Transactions on Antennas and Propagation* **14**, 302–307 (May 1966).
[44] Smit, J., Cilliers, J., and Burger, E., "Comparison of MLFMM, PO and SBR for RCS investigations in radar applications," in [*IET International Conference on Radar Systems (Radar 2012)*], **1**, 1–5, Institution of Engineering and Technology (IET) (October 2012).
[45] Chung, S. S. M. and Tuan, S.-C., "Comparison of NASA Almond Radar Cross Section Simulation Results from Shoot-Bouncing-Ray Method and Multi-Level-Fast-Multipole-Method," in [*2020 International Workshop on Electromagnetics: Applications and Student Innovation Competition (iWEM)*], Chiou, T.-W., ed., **1**, 36–37, Institute of Electrical and Electronics Engineers (IEEE) (August 2020).
[46] Schroder, A., Renker, M., Aulenbacher, U., Murk, A., Boniger, U., Oechslin, R., and Wellig, P., "Numerical and experimental radar cross section analysis of the quadrocopter DJI Phantom 2," in [*2015 IEEE Radar Conference*], **1**, 463–468, Institute of Electrical and Electronics Engineers (IEEE) (October 2015).
[47] Guay, R., Drolet, G., and Bray, J. R., "Measurement and modelling of the dynamic radar cross-section of an unmanned aerial vehicle," *IET Radar, Sonar & Navigation* **11**, 1155–1160 (May 2017).
[48] Studio, C. M., "CST Studio suite," (2010).
[49] Davidson, D. B., Theron, I. P., Jakobus, U., Landstorfer, F. M., Meyer, F. J., Mostert, J., and Van Tonder, J. J., "Recent progress on the antenna simulation program FEKO," in [*Proceedings of the 1998 South African Symposium on Communications and Signal Processing-COMSIG'98 (Cat. No. 98EX214)*], 427–430, Institute of Electrical and Electronics Engineers (IEEE) (September 1998).
[50] Homsup, N. and Breakall, J., "Application of XFDTD and FEKO program to the analysis of planar antennas," in [*2010 10th International Symposium on Communications and Information Technologies*], **2**, 646–650, Institute of Electrical and Electronics Engineers (IEEE) (October 2010).
[51] ANSYS, I., "Ansys hfss for antenna simulation," (2014).
[52] Björklund, S. and Hernnäs, H., "Statistical analysis of the RCS of a small fixed-wing UAV during a typical flight," in [*International Conference on Radar Systems (RADAR 2022)*], Balleri, A. and Clemente, C., eds., **2022**, 512–517, Institution of Engineering and Technology (IET) (October 2022).
[53] Björklund, S. and Hernnäs, H., "Statistical analysis of the radar cross section of two small fixed-wing drones using typical flights," *IET Radar, Sonar & Navigation* **18**, 125–136 (January 2024).
[54] Brooker, G. M., "Mutual Interference of Millimeter-Wave Radar Systems," *IEEE Transactions on Electromagnetic Compatibility* **49**(1), 170–181 (2007).
[55] Savage-Leuchs, M., Eisenberg, E., Liu, A., Henrie, J., and Bowers, M., "High-pulse energy extraction with high peak power from short-pulse eye safe all-fiber laser system," in [*Fiber Lasers III: Technology, Systems, and Applications*], Brown, A. J. W., Nilsson, J., Harter, D. J., and Tünnermann, A., eds., **6102**, 610207, International Society for Optics and Photonics, SPIE (February 2006).
[56] Yang, H., Wu, L., Wang, X., Shi, J., Li, G., and Ji, X., "Evaluation of beam quality for high-power lasers," in [*High-Power Lasers and Applications IV*], Fan, D. and Walter, R. F., eds., **6823**, 682316, International Society for Optics and Photonics, SPIE (February 2008).
[57] Slater, J., "Characterization of High-Power Lasers," *Journal of Directed Energy* **4**, 168–188 (Winter 2010).

[58] Bukharskii, N. D., Vais, O. E., Korneev, P. A., and Bychenkov, V. Y., "Restoration of the focal parameters for an extreme-power laser pulse with ponderomotively scattered proton spectra by using a neural network algorithm," *Matter and Radiation at Extremes* **8**, 014404 (December 2022).

[59] Ward, D., Sanyal, S., Vo, T., Bowers, J., Fiorino, S., and Flores, N., "High Energy Laser Measurements Using Beam Irradiance on Target System (BITS) with In-situ Primary Standard," *Journal of Directed Ebergy* **7** (Spring 2023).

[60] Kukreja, V., Moshman, N., Sritharan, S., and DeGrassie, J., "Inversion methods for laser parameter extraction with phenomenological model based on off-axis sensor measurements," *Inverse Problems in Science and Engineering* **24**, 604–624 (June 2016).

[61] McClatchey, R. A. and D'Agati, A. P., "Atmospheric Transmission of Laser Radiation: Computer Code LASER," Tech. Rep. ADA056659, Air Force Geophysics Lab HANSCOM AFB MA, United States (January 1978).

[62] Crawford, D. P., Sigal, E. J., Tyson, R. K., and Morgan, R. J., "Ground-based laser atmospheric propagation analysis–the Omega code," in [*Propagation of High-Energy Laser Beams Through the Earth's Atmosphere*], Ulrich, P. B. and Wilson, L. E., eds., **1221**, 132–145, International Society for Optics and Photonics, SPIE (May 1990).

[63] Mehta, N. C., "GRAND: a 4-D wave optics code for atmospheric laser propagation," in [*Propagation Engineering: Fourth in a Series*], Bissonnette, L. R. and Miller, W. B., eds., **1487**, 398–409, International Society for Optics and Photonics, SPIE (July 1991).

[64] Sprangle, P., Peñano, J., Ting, A., Hafizi, B., and Gordon, D., "Propagation of Short, High-Intensity Laser Pulses in Air," *Journal of Directed Energy* **1**, 73–92 (Fall 2003).

[65] Steinhorst, R. K., "Book Review: Prodas 3.2, Conceptual Software," (1988).

[66] Fischer, M. and Hathaway, W., "Aeroballistic Research Facility Data Analysis System (ARFDAS)," Tech. Rep. AFATL-TR-88-48, US Air Force Armament Laboratory, Eglin Air Force Base, FL (1988).

[67] Wey, P., Corriveau, D., Saitz, T. A., de Rujiter, W., and Strömbäck, P., "BALCO 6/7-DoF Trajectory Model," in [*29th International Symposium on Ballistics*], Woodley, C. and Cullis, I., eds., National Defense Industrial Association (NDIA) and International Ballistics Society (IBS), Destech Publications (May 2016).

APPENDIX A. NOMENCLATURE

Nomenclature

HEL

Symbol	Description	Units
α	Fitting constant	–
$\mathcal{H}_m(x)$	Order m Hermitte polynomial	–
ω_0	Beam radius at the beam waist	m
ρ_0	Radial coherence length	m
$\Theta_{\text{atmosphere}}$	Angular spread due to atmospheric propagation	rad
Θ_{blooming}	Blooming-induced spread	rad
Θ_{diff}	Angular spread of a diffraction-limited Gaussian beam	rad
Θ_{jitter}	Angular spread due to beam jitter	rad
Θ_{spread}	Angular spreading	rad
$\Theta_{\text{turbulence}}$	Turbulence-induced spread	rad
Θ_{M^2}	Angular spread of higher order modes	rad
C_N^2	Refractive index structure coefficient	$\text{m}^{-2/3}$
C_B	Fitting constant	–
$I(x,y,z)$	Time-averaged HEL irradiance intensity	Wm^2
I_0	HEL peak irradiance	Wm^2
k	Fitting constant	–
L_0	Outer turbulence scale size	m
l_0	Inner turbulence scale size	m
M^2	Beam quality factor	–
P_{HEL}	HEL power	W
t_{dwell}	Laser dwell time	s
$w^2(x)$	Time-averaged laser spot size	m
x	Orthogonal coordinates axis	–
y	Orthogonal coordinates axis	–
z	Normal to the plane defined by x and y axes	–
z_c	Length scale	–
z_i	Length scale	–

Kinetic

Symbol	Description	Units
$\boldsymbol{\alpha}_e$	Yaw of repose vector	rad/s
$\boldsymbol{\Lambda}$	Coriolis acceleration	$\mathrm{m/s^2}$
$\boldsymbol{g}$	Gravity acceleration	$\mathrm{m/s^2}$
$\boldsymbol{v}_{\mathrm{proj}}$	Projectile's velocity	m/s
$\boldsymbol{x}_{\mathrm{proj}}$	Projectile's position	m
$\boldsymbol{x}_{\mathrm{wind}}$	Wind velocity	m/s
ρ	Medium density	$\mathrm{kg/m^3}$
$C_{\text{Mag-f}}$	Magnus force coefficient	–
C_{spin}	Spin damping coefficient	–
C_{D_0}	Mach number-dependent projectile drag coefficient	–
$C_{D_{\alpha^2}}$	Induced drag force coefficient	–
C_{L_α}	Lift force coefficient	–
$C_{L_{\alpha^3}}$	Cubic lift force coefficient	–
$C_{M_{\alpha^3}}$	Cubic overturning moment coefficient	–
C_{M_α}	Overturning moment coefficient	–
d	Projectile's calibre	m
I_x	Axial inertia moment	$\mathrm{kgm^2}$
m_{proj}	Projectile's mass	kg
p	Angular velocity of the spinning motion	rad/s
S_{proj}	Projectile's surface	$\mathrm{m^2}$
v_{50}	Ballistic limit or limit velocity	m/s

RADAR

Symbol	Description	Units
λ	Wavelength	m
$\mathcal{G}_{\mathrm{RX}}$	Antenna transmitter gain	dB
$\mathcal{G}_{\mathrm{TX}}$	Antenna receiver gain	dB
$\mathcal{P}_{\mathrm{TX}}$	Emitted power	W
$\Pr(\text{detection})$	Detection probability	–
$\Pr(\text{false alarm})$	False alarm probability	–
B	Instantaneous bandwidth	Hz

C	Fitting constant	–
F	Receiver noise figure	dB
K	Swerling case	–
k_B	Boltzmann constant	J/K
n_{pulses}	Number of pulses	–
R_{max}	Maximum detection range	m
T_0	Standard temperature	K
X_∞	Fitting constant	–
X_{SNR}	SNR random variable	–
MDS	Minimum detectable signal	W
SNR	Signal to noise ratio	–

UAV

Symbol	**Description**	**Units**
$\{\mathcal{E}_{\text{mission}}\}$	Energy density thresholds	J/m^3
σ	Radar cross section	cm^2